Coregistration of FDG PET and MRI of the Head and Neck Using Normal Distribution of FDG

Hidemasa Uematsu, Norihiro Sadato, Yoshiharu Yonekura, Tatsuro Tsuchida, Satoshi Nakamura, Katsuya Sugimoto, Atsuo Waki, Kazutaka Yamamoto, Nobushige Hayashi and Yasushi Ishii
Department of Radiology and Biomedical Imaging Research Center, Fukui Medical University, Fukui, Japan

For better localization of head and neck structures by PET with 2-^{18}F-2-deoxy-D-glucose (FDG), direct incorporation of anatomical information from MRI by the coregistration of FDG PET and MRI without external markers is proposed. **Methods:** Seventeen patients with neoplasms and 16 normal subjects who had both FDG PET and MRI were studied. First, the three-dimensional normal distribution of FDG was evaluated, and then the structures of the head and neck regions with normal distribution patterns of FDG were used as internal markers for the coregistration of PET and MRI. The effectiveness of the coregistration was evaluated using focal neoplasms that were identified by both PET and MRI as fiducial internal markers. **Results:** The normal structures selected as internal landmarks for coregistration were the tonsils, salivary glands, mucosal layers of the oral cavity and pharynx, spinal cord, inferior portion of the frontal lobe, cerebellum and nasal turbinates. These structures were more easily observed in sagittal or coronal sections than in transaxial sections. All primary neoplasms were delineated by PET, whereas 4 were missed by MRI. Thirteen primary tumors and 7 cervical lymph node metastases coregistered well, with a center-of-mass distance of <2 mm, whereas 10 lymph node metastases were slightly misregistered, with a center-of-mass distance of 7.8 ± 6.5 mm (mean ± s.d.), probably due to differences in neck positions. **Conclusion:** Normal distribution of FDG uptake in the head and neck regions delineated by multidirectional sections is important for effective coregistration of FDG PET with MRI.

Key Words: coregistration; head and neck neoplasms; FDG; PET; MRI

J Nucl Med 1998; 39:2121–2127

Positron emission tomography with 2-[^{18}F]fluoro-2-deoxy-D-glucose (FDG) is an established technique for measuring in vivo tissue glucose metabolism. FDG PET is highly sensitive in the detection of extracranial head and neck neoplasms (*1–7*). Recently, FDG PET was used for screening patients suspected of head and neck neoplasms (*1*) to detect tumor recurrence (*2*) and lymph node metastases (*3*) and to evaluate the response to radiation (*4,5*) or chemotherapy (*6*). Because there is considerable overlap of FDG uptake between normal structures and malignant lesions (*1*), knowledge of FDG accumulation in the normal structures is essential to avoid false-positive results in the interpretation of FDG PET in patients with malignant tumors (*8*). Direct incorporation of anatomical information from MRI to PET is also feasible for localization of the neoplasms. In this context, Jabour et al. (*9*) studied FDG uptake in the extracranial normal head and neck structures using transaxial PET images, with reference to nonregistered magnetic resonance images. They showed that nasal mucosa, gingiva, lymphoid tissue and salivary glands had relatively high FDG uptake. With the recent development of high-resolution PET, it has become possible to delineate normal structures more accurately.

The purpose of this study was to coregister PET images with corresponding magnetic resonance images, using structures with normal distribution of FDG uptake as anatomical landmarks and localizing the abnormal accumulation of FDG on the corresponding MRI. The normal distribution of FDG was evaluated in subjects with no known pathology in the head and neck regions. PET-MRI coregistration was performed on patients with head and neck tumors. Regions of high FDG uptake in the primary tumors and metastatic lesions were used as the landmarks for evaluating the effectiveness of coregistration.

MATERIALS AND METHODS

Thirty-three subjects (19 men, 14 women; age range 48–87 yr) were included in this retrospective study. Sixteen had been included in another research protocol for FDG PET studies and had no known malignancies in the head and neck area. The other 17 had FDG PET for the evaluation of their head and neck tumors, all of which were primary malignant tumors (squamous cell carcinoma). The tumors involved the tongue (six tumors), the nasopharynx (three tumors), the gingiva (two tumors), the oral mucosa (two tumors), the submandibular gland (one tumor), the oral lip (one tumor), the maxillary sinus (one tumor) and the mandible (one tumor). None of the subjects were known to have diabetes. Written informed consent was obtained from all subjects.

PET Imaging

All subjects underwent FDG PET study after a 4-hr fast. FDG PET was performed with a high-resolution, whole-body PET scanner with an 18-ring detector arrangement (Advance; General Electric Medical Systems, Milwaukee, WI). The physical characteristics of the scanner have been described in detail by DeGrado et al. (*10*). In brief, the system permitted the simultaneous acquisition of 35 transaxial images with interslice spacing of 4.25 mm. Axial and transaxial resolution was 4.2 mm, allowing multidirectional reconstruction of the images without loss of resolution. The field of view (FOV) and pixel size of the reconstructed images were 256 and 2 mm, respectively. The patient's head was carefully positioned such that the midsagittal plane of the head was parallel to the camera's sagittal plane. A laser-beam pointer was used to define the midsagittal plane to minimize the skewing of the neck relative to the head. A 10-min transmission scan was acquired with a ^{68}Ge/^{68}Ga source for attenuation correction. After an intravenous bolus injection of ~370 MBq of FDG was administered, static scanning was performed for 20 min (from 40 to 60 min postinjection). Plasma glucose levels were measured in all subjects.

MRI

MR images were obtained in all subjects. A 1.5-T magnetic resonance system (Horizon; General Electric Medical Systems) was used to obtain axial T1-weighted spin-echo images [repetition time (TR, in msec)/echo time (TE, in msec)/number of excitations (NEX) = 333/10/3] and T2-weighted fast spin-echo images (TR/TE/NEX = 3500/88/2) (FOV, 22 cm × 16 cm; matrix size, 256 ×

Received Nov. 17, 1998; revision accepted Apr. 12, 1998.
For correspondence or reprints contact: Hidemasa Uematsu, MD, Department of Radiology, Fukui Medical University, 23 Shimoaizuki, Matsuoka-cho, Yoshida-gun, Fukui, 910-1193, Japan.

224), as well as sagittal and coronal T1-weighted spin-echo images (FOV, 22 cm × 22 cm; matrix size, 256 × 224). Slice thickness was 4 mm, and slice interval was 1 mm. The 17 patients with head and neck tumors underwent contrast enhancement studies with intravenous administration of 0.1 mmol/kg body weight of gadopentetate dimeglumine (Magnevist; Nihon Schering, Osaka, Japan). The patient's head was carefully positioned, as they were in PET imaging. Height of the occipital pole from the examination table for MRI and PET was similar (PET, 5 cm; MRI, 5.5 cm).

Image Interpretation for Normal Distribution of FDG

Transaxial, sagittal and coronal PET images of all 33 subjects were inspected visually on a computer display monitor. Data from the 16 normal subjects were used to define the distribution of FDG accumulation in normal structures with reference to the anatomical MRI. Data from the patients were used to calculate the standardized uptake values (SUVs) of normal structures. A Hewlett Packard (Palo Alto, CA) Apollo 9000 Model 735 workstation served as an image display and analysis station. All operations were performed through a graphical user interface (Advance PET Imaging System). Axial, sagittal and coronal MR images were reviewed on film by visual inspection. FDG distribution in the normal structures was determined with reference to the anatomical information obtained by nonregistered MRI. Irregularly shaped regions of interest (ROIs) were drawn to encompass the whole area of each normal structure for quantification of FDG uptake. If the normal structure was too close to malignant tissue, ROIs analysis was not performed on that structure. The mean SUVs were determined as follows:

$$\text{SUV} = \frac{\text{Radioactivity in ROI (Bq/cm}^3\text{)}}{\text{Injected dose (Bq)/body weight (g)}}.$$

We observed the distribution of FDG in normal structures, comparing each level of the PET images with the corresponding nonregistered MR images. These images were evaluated by two radiologists. In seven subjects, the concentration of radioactivity in saliva was measured directly by a well counter and the weight of the sample, not from PET images. The SUV of saliva was calculated by the formula given above.

Coregistration of FDG PET and MRI

Image registration was performed in the 17 patients, who each had a primary malignant tumor. These patients had a total of 17 FDG-positive lymph nodes. The pathological confirmation was established in all primary tumors but was not available for the lymph nodes. Because the sensitivity and specificity for detecting lymph node involvement of the head and neck are 90% and 96%, respectively, for FDG PET (*1*), lymph nodes with a positive FDG accumulation were considered to be metastases.

MRI and FDG PET datasets were transferred to a SUN workstation (SPARCstation MP20; SUN Microsystems, Mountain View, CA). The final voxel sizes of the MRI and FDG PET images were 0.86 × 0.86 × 5 mm and 4.2 × 4.2 × 4.25 mm, respectively. Image registration was performed on a SUN workstation using a software package (Dr. View; Asahi Kasei Joho System Co., Ltd., Tokyo, Japan). This image registration method has been described in detail by Kapouleas et al. (*11*) for coregistration of brain structures. This approach splits the three-dimensional problem into two two-dimensional problems. First, the three-dimensional position and orientation of the midsagittal plane were determined for both the PET and MRI volumes. Midsagittal lines in the transaxial images of both MRI and PET were aligned manually. Midsagittal planes were fitted with the least squares method to the set of the midsagittal lines. Both PET and MRI volumes were then resliced parallel to the midsagittal planes. Second, the sagittal PET sections were aligned manually with the corresponding resliced MR sagittal sections. The internal markers used for the first step included the tonsils, salivary glands, cerebellar hemisphere and spinal cord on the transaxial slices. The second step used the mucosal surface of the oral and pharyngeal wall, lips, bases of the cerebellar hemispheres, inferior frontal lobe and spinal cord on the midsagittal section. The observer can freely adjust the color scale and intensity of the PET images to optimize the visualization of normal structures. Superimposed PET images on MR images were displayed in pseudocolor display, whereas MR images remained in gray-scale display.

The efficacy of the coregistrations was assessed using patients with tumors that showed focal FDG uptake by PET and mass formation by MRI. These tumors were used as internal fiducial markers because the normal structures were used to estimate the transform parameters for coregistration. The degree of misregistration of the neoplasms was evaluated with the following criteria: when the distance between the center of gravity of FDG accumulation and the corresponding mass on the MR image was <2 mm, the mass was considered to be coregistered. Anything greater than this threshold was considered a misregistration.

Criteria for grading coregistration were as follows: both the primary tumor and lymph node were coregistered (Grade 1); the primary tumor was coregistered without lymph node metastases depicted by FDG (Grade 2); the primary tumor was coregistered and lymph node metastases were misregistered (Grade 3); the primary tumor was misregistered and lymph node metastases were coregistered (Grade 4); the primary tumor was misregistered without lymph node metastases depicted by FDG (Grade 5); and both the primary tumor and lymph node metastases were misregistered (Grade 6). This grading system is a reasonable one for evaluating the effectiveness of coregistration because the grade was determined by the degree of coregistration of multiple markers (in this case, primary tumors and distant lymph nodes). This is particularly useful in the head and neck regions, to which a rigid-body assumption cannot be applied.

RESULTS

FDG Distribution in High-Resolution PET Images

Typical FDG PET images and the corresponding nonregistered magnetic resonance images are shown in Figures 1–4. The results of FDG uptake on the normal head and neck structures are summarized in Table 1. The tongue surface was well visualized, whereas the tongue muscle showed lower FDG uptake on the midsagittal section (Fig. 1, upper). The mucosa of the pharyngeal wall (nasopharynx, oropharynx and hypopharynx), nasal turbinates, lips, spinal cord and cerebellum were also well visualized on the midsagittal FDG PET image (Fig. 1, upper). On the transaxial image through the oropharynx, the gingiva of the oral cavity and parotid glands showed increased activity (Fig. 2, left). The palatine tonsils showed bilaterally paired increased activity on the axial image through the oropharynx (Fig. 2, left). On the transaxial image through the lingual radix, the submandibular and sublingual glands were well visualized (Fig. 3, left). The palatine and lingual tonsils (Waldyer's ring) showed a U-shaped increase of activity on the coronal image (Fig. 4, upper). In the hypopharyngeal region, the mucosa of the pyriform sinus was well visualized on the coronal image (Fig. 4, upper). These structures showed higher activity than striate muscle or bone. The thyroid gland, striate muscle and bone showed less FDG uptake. The radioactivity of saliva was negligible (SUV = 0.13 ± 0.11, mean ± s.d., converted from radioactivity concentration to SUV). The plasma glucose level of these subjects ranged from 74 to 120 mg/dl. No

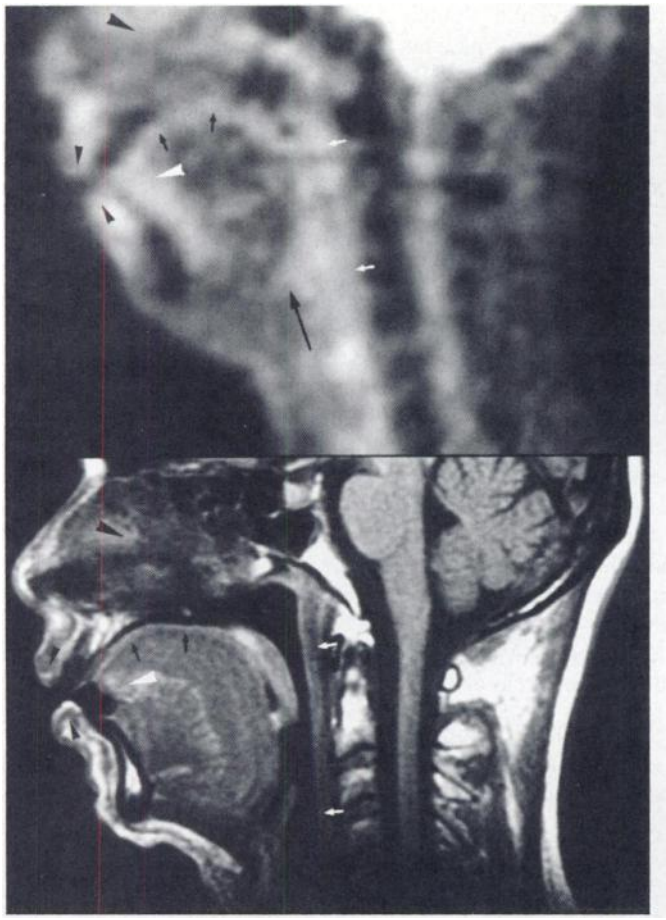

FIGURE 1. Midsagittal section of normal FDG PET (upper) and corresponding MR image (lower). Tongue surface (small black arrows), lips (small black arrowheads), nasal turbinates (large black arrowhead), mucosa of pharyngeal wall (nasopharynx, oropharynx and hypopharynx, small white arrows), cerebellum and spinal cord were well visualized by FDG PET. High FDG uptake in floor anterior to tongue (white arrowhead) indicates mucosal folding between tongue and gingiva, and that in lingual radix (large black arrow) corresponds to lingual tonsils, lingual mucosa and oropharyngeal mucosa.

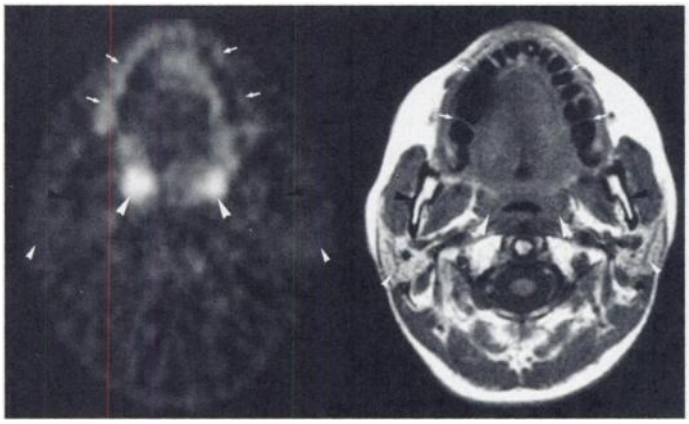

FIGURE 2. Transaxial section of normal FDG PET through region of oropharynx (left) and corresponding MR image (right) at slightly different angles. Gingiva of oral cavity (small white arrows) and palatine tonsils (large white arrowheads) show increased activity. Parotid glands are low in activity in this subject (small white arrowheads). Mandibular bone shows negligible activity (black arrowheads).

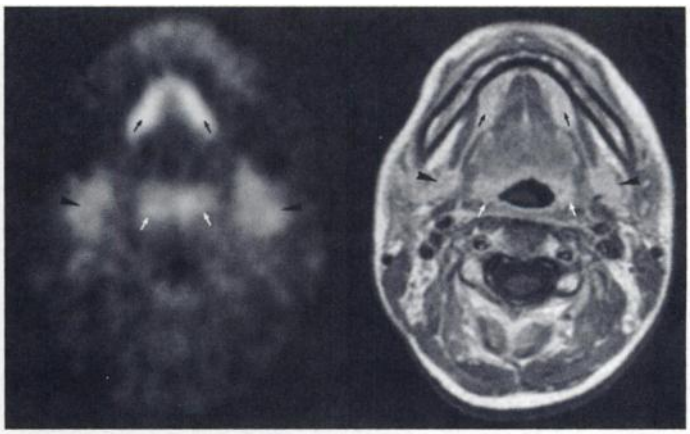

FIGURE 3. Transaxial FDG PET image through lingual radix (left) and corresponding MR image (right) at slightly different angles. Submandibular glands (black arrowheads) show high FDG uptake. Reversed-V-shaped FDG uptake in oral floor (black arrows) corresponds to sublingual glands. High FDG uptake in lingual radix (white arrows) corresponds to the lingual tonsils, with possible contribution from mucosa of lingual radix.

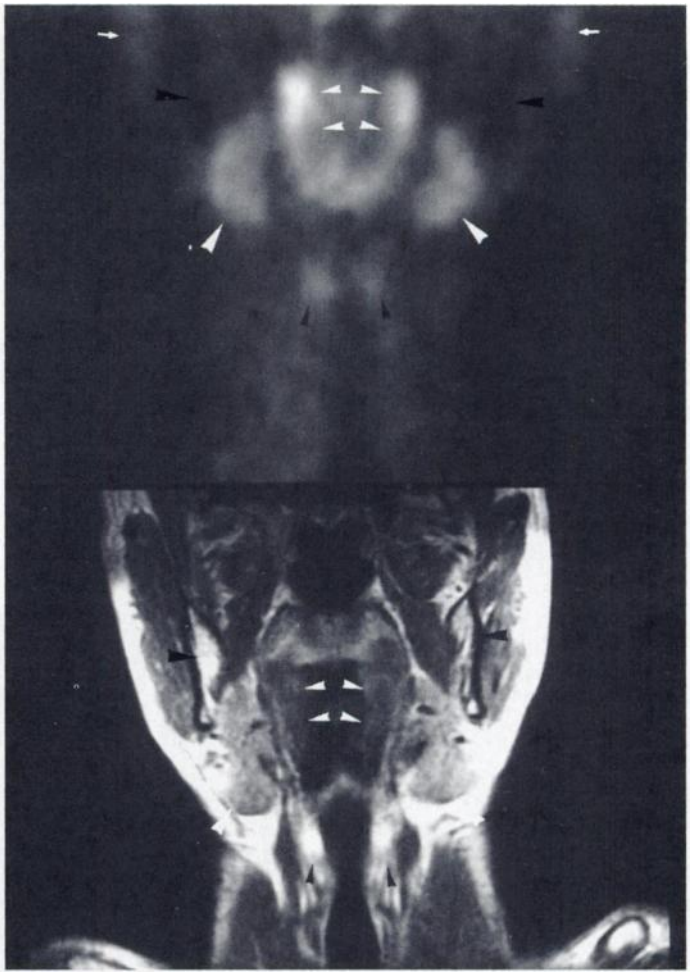

FIGURE 4. Coronal section of FDG PET (upper) and corresponding MR image (lower) through region of pharynx. U-shaped FDG uptake in pharynx (small white arrowheads) corresponds to palatine and lingual tonsils (Waldyer's ring). Submandibular glands (large white arrowheads) and parotid glands (white arrows) show high FDG uptake. Mucosa of pyriform sinus was well visualized (small black arrowheads). Masseter muscles and pterygoid muscles, as well as mandibular bone (large black arrowheads) show negligible activity.

TABLE 1
Results of FDG Activity in Normal Structures

Structure	SUV*(mg/ml)	Sample size†
Palatine tonsils	4.22 ± 1.31	31
Lingual tonsils	3.67 ± 0.99	31
Lips	3.38 ± 1.57	29
Sublingual glands	3.00 ± 1.47	33
Soft palate	2.43 ± 0.67	32
Tongue surface	2.28 ± 0.72	32
Gingiva	2.21 ± 0.73	33
Spinal cord	2.09 ± 0.56	33
Hypopharynx	2.07 ± 0.54	33
Nasal turbinates	1.99 ± 0.79	31
Nasopharynx	1.94 ± 0.57	30
Submandibular glands	1.89 ± 0.66	33
Oropharynx	1.89 ± 0.51	33
Parotid glands	1.43 ± 0.49	33
Saliva	0.13 ± 0.11	7

*Values are mean ± s.d.
†Sample size was less than the total number of patients because primary tumors were in the respective anatomical structures or out of scan range. The radioactivity of saliva was converted to a SUV.
SUV = standardized uptake value.

correlation was observed between the plasma glucose level and SUV in each region.

Coregistration of FDG PET and MRI

Primary tumor size varied from 15 × 15 mm to 40 × 40 mm in diameter, as defined by MRI. All 17 primary malignant tumors were clearly delineated with PET, whereas 4 were missed by MRI. The time required for alignment of FDG PET and MRI was <1 hr for each subject. In 13 patients, all primary tumors were coregistered (Table 2). Four patients with seven coregistered lymph nodes were classified as Grade 1. Five patients without lymph node metastases were classified as Grade 2. Four patients with 10 misregistered lymph node metastases (7.8 ± 6.5 mm, mean ± s.d., in distance of center of gravity) were classified as Grade 3. Typical coregistration images are shown in Figures 5–7.

DISCUSSION

Diagnostic Value of Coregistration

Many studies (*1–7*) have addressed the issue of the uptake of FDG in malignant head and neck tumors. A study on the uptake of FDG in relation to the proliferation rate of squamous cell carcinomas of the head and neck (*12*) showed that the glucose uptake correlated with the proliferative activity of the tumor or metastases. However, it has been shown (*1*) that FDG uptake is extremely variable in primary tumors (SUV = 2.0–13.8) and lymph node metastases (SUV = 1.4–11.4). These results suggest that there is a large overlap between lesions and normal structures. Furthermore, it has been reported (*13*) that FDG accumulates not only in malignant tumors but also in inflammatory lesions. An advantage of coregistration in this issue is that it can depict FDG uptake in the particular structures identified by MRI. Hence, coregistration is useful for differentiation between lesions and normal structures.

Normal Distribution of FDG

In this study, we observed the distribution of FDG in the head and neck region with good resolution on axial, coronal and sagittal sections. In agreement with the report of Jabour et al. (*9*), the FDG uptake was relatively high in the nasal turbinates, cerebellum, gingiva, tonsils and salivary glands. Furthermore, the tongue surface, mucosa of the pharyngeal wall, spinal cord and lips were particularly well-visualized on coronal and sagittal sections (Figs. 1–4).

When the size of the structure of interest is smaller than about twice the FWHM, the FDG activity in the structure is under-

TABLE 2
Patient Characteristics and Coregistration of FDG PET and MR Images

Patient no.	Age	Sex	Clinical diagnosis	Tumor size*	MRI findings†	Lymph node metastases‡			Image registration§
						FDG uptake	PET (R/L)	MRI (R/L)	
1	73	M	Tongue cancer	30 × 10	Positive	Positive	−/+	−/+	Grade 1
2	59	M	Gingival cancer	30 × 20	Positive	Positive	−/+	−/+	Grade 1
3	68	M	Oral mucosal cancer	20 × 20	Positive	Positive	−/++	−/++	Grade 1
4	75	F	Maxillary cancer	18 × 14	Positive	Positive	+/++	+/++	Grade 1
5	52	M	Tongue cancer	40 × 40	Positive	Positive	−/−	−/−	Grade 2
6	73	M	Nasopharyngeal cancer	40 × 20	Positive	Positive	−/−	−/−	Grade 2
7	62	M	Nasopharyngeal cancer	20 × 20	Positive	Positive	−/−	−/−	Grade 2
8	72	M	Gingival cancer	28 × 21	Positive	Positive	−/−	−/−	Grade 2
9	52	M	Mandible cancer	40 × 30	Positive	Positive	−/−	−/−	Grade 2
10	73	F	Tongue cancer	15 × 15	Positive	Positive	+/−	+/−	Grade 3
11	75	M	Tongue cancer	40 × 20	Positive	Positive	++/++	++/++	Grade 3
12	63	M	Oral mucosal cancer	20 × 20	Positive	Positive	−/++++	−/++++	Grade 3
13	58	F	Submandibular gland cancer	30 × 30	Positive	Positive	+/−	+/−	Grade 3
14	68	M	Tongue cancer	—	Negative	Positive	−/−	−/−	—
15	87	F	Tongue cancer	—	Negative	Positive	−/−	−/−	—
16	62	M	Nasopharyngeal cancer	—	Negative	Positive	−/−	−/−	—
17	48	M	Oral lip cancer	—	Negative	Positive	−/−	−/−	—

*Estimated by MRI (in mm).
†Positive = detected; negative = not detected.
‡Lymph node metastases on PET and MRI of both sides of neck (− = no suspicious nodes; + = one suspicious node; ++ = two suspicious nodes; +++ = three suspicious nodes; ++++ = four or more suspicious nodes).
§— = tumors were not delineated by MRI.
R = right; L = left.

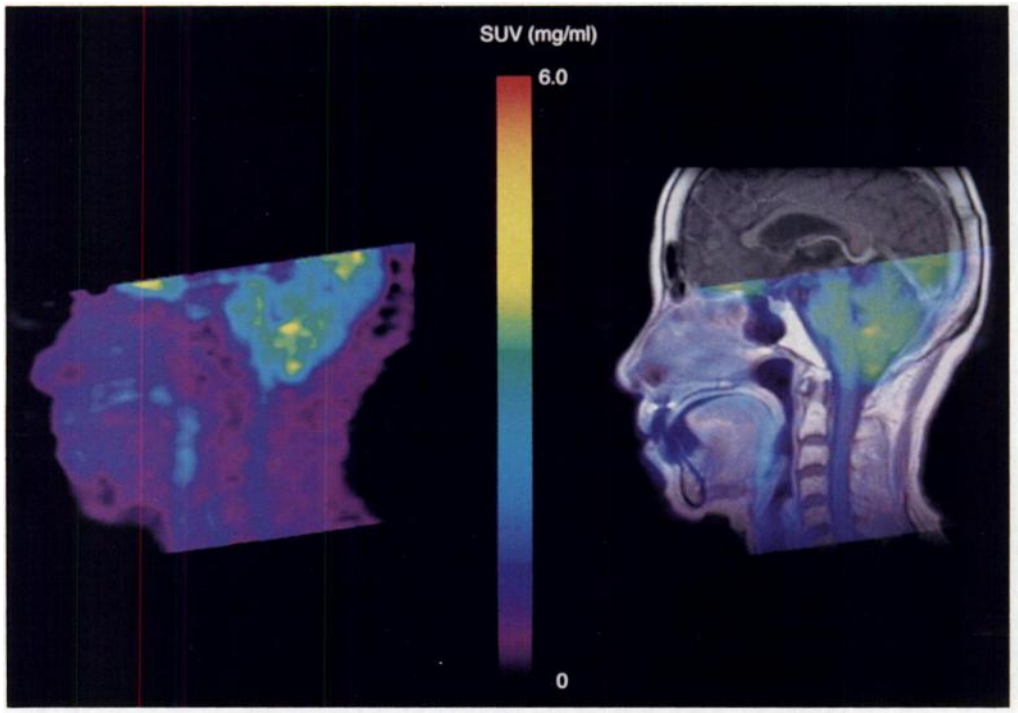

FIGURE 5. Midsagittal section of FDG PET (left) and its overlay on coregistered MR image (right; Patient 4). In merged image, MRI is in gray-scale and FDG PET is in pseudocolor scale. Normal structures that were well visualized by both FDG PET and MRI, such as mucosal surface of oral and pharyngeal wall, lips, cerebellar hemisphere, inferior frontal lobe and spinal cord, were used for coregistration.

estimated. In this study, the FWHM of a reconstructed FDG PET image was ~4.2 mm. The ROIs of almost all the normal structures were less than twice the FWHM in diameter. Hence, a partial volume effect should be considered in the quantification of the radiotracer. On the other hand, the distribution and localization of the radioactivity, which are essential components of this study, are minimally affected.

Accumulation of FDG in the oral and pharyngeal cavities has not been well described, probably because it is less clearly visualized in transaxial images than in coronal and sagittal images. Because the radioactivity of saliva was negligible (*9*), FDG should be distributed in the metabolically active mucosa.

The palatine and lingual tonsils (Waldyer's ring) showed a high accumulation of FDG, which is consistent with the article by Jabour et al. (*9*) and probably reflects the high metabolic activity necessary for mitosis of lymphocytes (*14*).

The salivary glands (sublingual, submandibular and parotid) showed FDG accumulation, which is also consistent with the report by Jabour et al. (*9*). Because the parenchymal elements of the salivary glands are derived from the oral epithelium (*15*), the salivary glands, as well as the oral and pharyngeal mucosa, may be metabolically active.

In an early PET study (*16*), accumulation of FDG in the spinal cord was not fully evaluated because of the low spatial resolution of the PET camera, but recently, high-resolution PET has consistently delineated the cervical spinal cord (*17*). The spinal cord is a part of the central nervous system, which is supposed to be metabolically active (*18*).

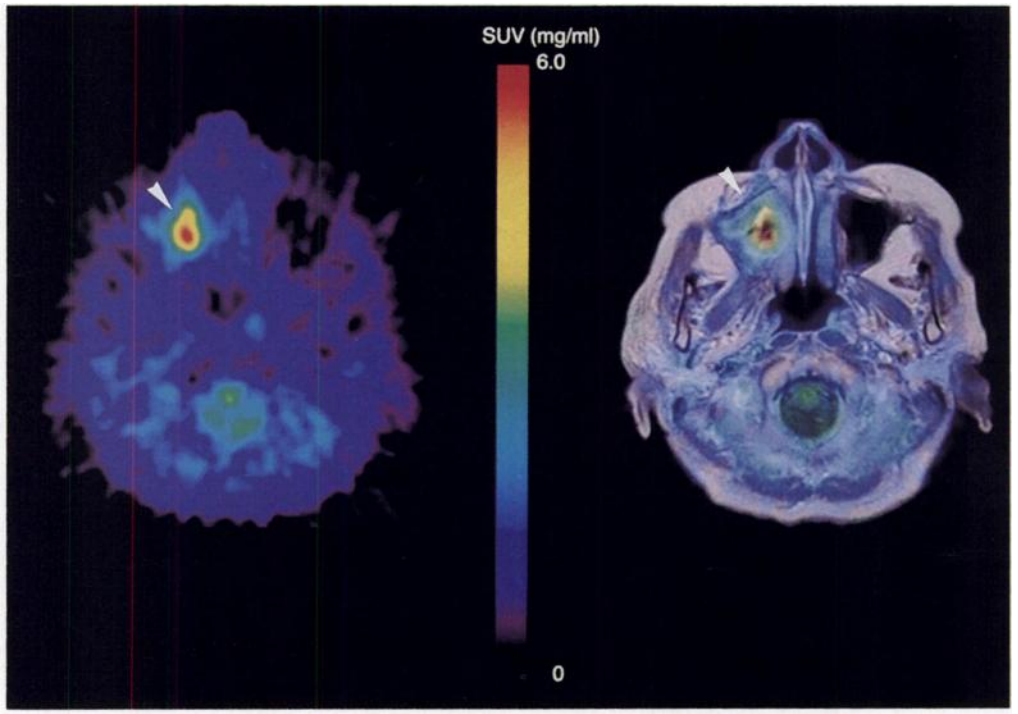

FIGURE 6. Transaxial FDG PET image of patient with maxillary cancer (left; Patient 4) and its overlay on coregistered MR image (right). Tumor size was 14 × 18 mm in diameter, as defined by MRI. High FDG uptake in primary tumor (white arrowhead) is well visualized.

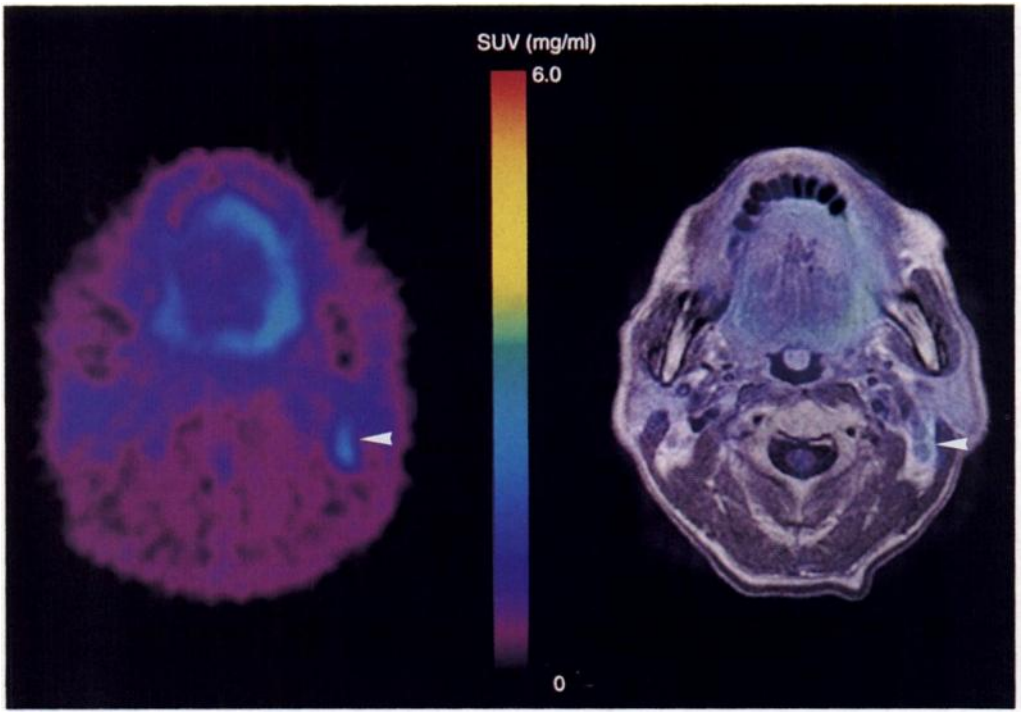

FIGURE 7. Transaxial FDG PET image of metastatic cervical lymphadenopathy (left) of patient with oral mucosal cancer (Patient 3) and its overlay on coregistered MR image (right). Two enlarged lymph nodes, 12 and 5 mm in diameter, respectively, medial to left sternocleidomastoid muscle (white arrowhead) show high FDG uptake.

Coregistration of FDG PET and MRI

MRI can provide detailed anatomical information, which aids clinical staging and therapeutic planning. The advantages of MRI are high contrast between diseased and normal tissue and the ability to show coronal and sagittal images directly (*19*).

Recently, several approaches have been suggested for anatomical alignment between different modalities. For example, the use of three-dimensional surface fitting (*20–23*), external fiducial markers (*22,23*) or internal fiducial markers (*24,25*) was proposed. Although surface fitting was shown to be successful in brain studies (*20*), surface detection would be a problem in the nonbrain head and neck region. Patients' measurements with external markers visible in SPECT and MRI or CT would provide some indication of quality of fit at the surface but may not indicate the accuracy of registration for deep structures (*21*). The reproducibility of the marker location would also be a problem if the two examinations were performed on separate days. The use of internal landmarks and, particularly, three-dimensional dataset fitting has the advantages of both improved matching accuracy and convenience (*24*)

Wong et al. (*25*) validated the usefulness of coregistration of FDG PET and CT or MRI in the head and neck region. They showed that point-like landmarks that had negligible FDG uptake, such as the cervical spinous process, tip of the odontoid peg, centrums of facet joints and centrums of globes and fillings were suitable for internal markers. Compared with these point-like markers of mainly bones, with negative contrast with adjacent structures, the internal landmarks proposed in this study represent positive contrast, as well as characteristic features of large soft tissue structures, such as the tongue or spinal cord, and are easily recognized by multidirectional sections. Whereas a negative marker would be beneficial for coregistration of PET with CT, which depicts bone well, a positive marker may be useful with MR, which delineates soft tissue structures.

The proposed method precisely coregistered FDG accumulation in the primary tumors with the corresponding mass depicted by MRI. On the other hand, more than half of the cervical lymph node metastases were misregistered, although the degree of misregistration was relatively small (<15 mm). This may be partly due to differences of subtle neck flexion and rotation during the MRI and FDG PET studies. Our method is based on the assumption of a rigid body, which is satisfied by the head but not by the neck. Hence, coregistration is less accurate in the neck region. The process we used in this study is strictly the same as that described by Kapouleas et al. (*11*) except for the landmarks, which were selected on the study of normal subjects. In applying our method, positioning of the head and neck is important. Positioning procedure of the head and neck for MRI and PET was similar: rotation around the caudal–rostral axis and around the dorsal–ventral axis relative to the scanner's axis and between head and neck were carefully eliminated by visual inspection and laser beam pointer. Although rotation around the right–left axis due to slight extension and flexion of the neck was not controlled completely, height of the occipital pole from the examination table for MRI and PET was kept similar (PET, 5 cm; MRI, 5.5 cm). Because of this careful positioning, coregistration with the assumption of a rigid body was fairly useful for localization of the increased uptake of FDG by metastatic lymph nodes, if MRI depicts them. A possible image registration technique to compensate the subtle misregistration due to extension–flexion of the neck would be nonlinear warping of the neck portion along the cervical spinal cord. The immobilization mask is one of the choices, if it is available. In our institution, however, a cast used for patients with planned radiotherapy cannot be held in the MR head coil; hence, we did not use it.

To evaluate the coregistration between different imaging modalities, fiducial markers that can be identified on both image modalities are necessary. Tumors instead of normal structures were used as fiducial internal markers because tumors usually show high FDG uptake by PET and mass formation by MRI and because we have used FDG distribution of normal structures to estimate the transform parameters; hence, normal structures cannot be used for their validation. Tumors may not be the ideal landmark for the evaluation of the accuracy of coregistration because they are not a point source

and subject to different signal intensity distribution due to the tumor heterogeneity of the magnetic resonance or PET signal. Despite this limitation, the center-of-mass distance was <2 mm, underscoring the accuracy of this method. This is probably due to the fact that the signal distribution of these particular tumors was relatively homogeneous because the tumors were relatively small (from 15 × 15 mm to 40 × 40 mm in diameter as defined by MRI) and the fact that the center of gravity is robust against the heterogeneity effect. Characteristics of these particular tumors do not affect the validity of the coregistration procedure because our method uses the normal structures not the tumors.

The grading system is for semiquantification of visual inspection using primary and metastatic lesions as internal fiducial markers. It is a reasonable approach to consolidate the accuracy of the measurement of each internal fiducial marker by the center-of-gravity distance because the grade was determined by the degree of coregistration of multiple markers. This is particularly useful in the head and neck regions, to which rigid-body assumption cannot be applied.

CONCLUSION

High-resolution PET with multisectional displays depicted normal FDG distribution in the head and neck region, which, in turn, allowed efficient coregistration of PET and MRI.

ACKNOWLEDGMENTS

We thank Masato Tanaka, RT, Department of Radiology, Fukui Medical University and Hideaki Hayashi, Asahi Kasei Joho System Co., Ltd., for assistance with image registration. This study was supported in part by the Research Grant JSPS-RFTF97L00203 for the "Research for the Future" Program from the Japan Society for the Promotion of Science.

REFERENCES

1. Laubenbacher C, Saumweber D, Wagner-Manslau C, et al. Comparison of fluorine-18-fluorodeoxyglucose PET, MRI and endoscopy for staging head and neck squamous-cell carcinomas. *J Nucl Med* 1995;36:1747–1757.
2. Lapera M, Grenman R, Kurki T, et al. Head and neck cancer: detection of recurrence with PET and 2-[F-18]fluoro-2-deoxy-D-glucose. *Radiology* 1995;197:205–211.
3. Braams JW, Pruim J, Freling NJ, et al. Detection of lymph node metastases of squamous-cell cancer of the head and neck with FDG-PET and MRI. *J Nucl Med* 1995;36:211–216.
4. Chaiken L, Rege S, Hoh C, et al. Positron emission tomography with fluorodeoxyglucose to evaluate tumor response and control after radiation therapy. *Int J Radiat Oncol Biol Phys* 1993;27:455–464.
5. Greven KM, Williams DW, Keyers JW, et al. Distinguishing tumor recurrence from irradiation sequelae with positron emission tomography in patients treated for larynx cancer. *Int J Radiat Oncol Biol Phys* 1994;29:841–845.
6. Reisser C, Haberkorn U, Dimitrakopoulou-Strauss A, et al. Chemotherapeutic management of head and neck malignancies with positron emission tomography. *Arch Otolaryngol Head Neck Surg* 1995;121:272–276.
7. Strauss LG, Conti PS. The application of PET in clinical oncology. *J Nucl Med* 1991;32:623–648.
8. Barrington SF, Maisey MN. Skeletal muscle uptake of fluorine-18-FDG: effect of oral diazepam. *J Nucl Med* 1996;37:1127–1129.
9. Jabour BA, Choi Y, Hoh CK, et al. Extracranial head and neck: PET imaging with 2-F-18 fluoro-2-deoxy-D-glucose and MR imaging correlation. *Radiology* 1993;186:27–35.
10. DeGrado TR, Turkington TG, Williams JJ, et al. Performance characteristics of a whole-body PET scanner. *J Nucl Med* 1994;35:1398–1406.
11. Kapouleas I, Alavi A, Alves WM, Gur RE, Weiss D. Registration of three-dimensional MR and PET images of the human brain without markers. *Radiology* 1991;181:731–739.
12. Haberkorn U, Strauss LG, Reisser C, et al. Glucose uptake, perfusion and cell proliferation in head and neck tumors: relation of positron emission tomography to flow cytometry. *J Nucl Med* 1991;32:1548–1555.
13. Kubota R, Yamada S, Kubota K, Ishikawa K, Tamahashi N, Ido T. Intra-tumoral distribution of fluorine-18-fluorodeoxyglucose in vivo: high accumulation in macrophages and granulation tissues studied by microautoradiography. *J Nucl Med* 1992;33:1972–1980.
14. Provenza DV. Tongue and tonsils. In: Provenza DV, ed. *Oral histology: inheritance and development*, 2nd ed. Philadelphia: Lea & Feiger; 1986:418–429.
15. Bhaskar SN. Salivary glands. In: Bhaskar SN, ed. *Orban's oral histology and embryology*. 8th ed. St. Louis: C.V. Mosby; 1976:328–360.
16. Di Chiro G, Oldfield E, Bairamian D, et al. Metabolic imaging of the brain stem and spinal cord: studies with positron emission tomography using 18F-2-deoxyglucose in normal and pathological cases. *J Comput Assist Tomogr* 1983;7:937–945.
17. Kamoto Y, Sadato N, Yonekura Y, et al. Visualization of cervical spinal cord with 18FDG and high resolution PET. *J Comput Assist Tomogr* 1998;22:487–491.
18. Phelps ME, Huang SC, Hoffman EJ, et al. Tomographic measurement of local cerebral glucose metabolic rate in humans with (F-18) 2-fluoro-2-deoxy-D-glucose: validation of method. *Ann Neurol* 1979;6:371–388.
19. Vogl T, Dresel S, Bilaniuk LT, et al. Tumors of the nasopharynx and adjacent areas: MR imaging with Gd-DTPA. *AJR* 1990;154:585–592.
20. Pelizzari CA, Chen GTY, Spelbring DR, Weichselbaum RR, Chen CT. Accurate three-dimensional registration of CT, PET, and/or MR images of the brain. *J Comput Assist Tomogr* 1989;13:20–26.
21. Holman BL, Zimmerman RE, Johnson KA, et al. Computer-assisted superimposition of magnetic resonance and high-resolution technetium-99m-HMPAO and thallium-201 SPECT images of the brain. *J Nucl Med* 1991;32:1478–1484.
22. Scott AM, Macapinlac H, Zhang J, et al. Image registration of SPECT and CT images using an external fiduciary band and three-dimensional surface fitting in metastatic thyroid cancer. *J Nucl Med* 1995;36:100–103.
23. Pietrzyk U, Herholz K, Fink G, et al. An interactive technique for three-dimensional image registration: validation for PET, SPECT, MRI and CT brain studies. *J Nucl Med* 1994;35:2011–2018.
24. Wahl RL, Quint LE, Cieslak RD, Aisen AM, Koeppe RA, Meyer CR. "Anatometabolic" tumor imaging: fusion of FDG PET with CT or MRI to localize foci of increased activity. *J Nucl Med* 1993;34:1190–1197.
25. Wong WL, Hussain K, Chevretton E, et al. Validation and clinical application of computer-combined emission tomography with 2-[18F]fluoro-2-deoxy-D-glucose head and neck images. *Am J Surg* 1996;172:628–632.

Erratum

The labeling of "p" and "i" in Figure 2C in the article, "Dual-Head Pinhole Bone Scintigraphy," by Bahk et al. (*JNM* 1998;39:1444–1448) was printed incorrectly. The correct labeling would be the reverse of how they are marked.